Journal of Catalysis **211,** 6–18 (2002)
doi:10.1006/jcat.2002.3708

# Isobutane/2-Butene Alkylation Using Large-Pore Zeolites: Influence of Pore Structure on Activity and Selectivity

Kyesang Yoo, Eric C. Burckle, and Panagiotis G. Smirniotis[1]

*Department of Chemical Engineering, University of Cincinnati, Cincinnati, Ohio 45221-0171*

Received March 1, 2001; revised May 21, 2002; accepted June 4, 2002

**The alkylation of isobutane with 2-butene was performed in the liquid phase at 80°C and 300 psi. This study constitutes a detailed comparison under identical conditions of 12-membered pore zeolites with different dimensionalities, namely USY, mordenite, beta, LTL, and ZSM-12 zeolite. Particular attention was paid to the role of the structural characteristics of the catalysts. In the mechanism studies, very-low-olefin feed (i/o molar ratio of 1000, olefin WHSV of 0.01 $h^{-1}$) was used to keep real alkylation without undesirable oligomerizations. For selectivity toward the individual TMP and DMH compounds, pore structure plays a significant role. At the initial stage (5 min on stream), it was found that the relative value for TMP selectivities described by the configurational ratio of 2,2,4-/2,2,3-TMP to 2,3,3-/2,3,4-TMP decreased in the following order: beta ≥ ZSM-12 > mordenite > USY ≥ LTL. Beta and ZSM-12 showed higher values due to their specific pore structure (the absence of large expansions at either the channel intersections or within the channel itself), in which bulky TMPs could diffuse out without structural restriction. In order to support this, the ratio of diffusivity for selected TMP isomers (2,2,4- to 2,3,4-TMP) was obtained. The value of diffusivity ratio of 2,2,4-TMP to 2,3,4-TMP decreased in the sequence beta > USY > LTL. This difference was reflected clearly in the different distribution of TMP isomers. The comparable trends were also observed for the selectivity of DMHs, ratio of 2,5-/2,4-/2,3-DMH to 3,4-DMH. Most of cracking products, 2-methyl butane, 2,3-dimethyl butane, and 2,3- and 2,4-dimethly pentane, were formed by type A β-scissions from $[C_{12}H_{25}]^+$ and $[C_{16}H_{33}]^+$. For other studies with different feed conditions (i/o molar ratio of 98, olefin WHSV of 0.1 $h^{-1}$), it was also observed that the pore structure of zeolites plays a significant role in the activity of olefin conversion. Beta and ZSM-12 were shown to outperform other zeolites because their favorable pore structures limited the accumulation of carbonaceous compounds that lead to pore plugging. This is in contrast to the common belief that three-dimensional zeolites are less susceptible to pore plugging than one-dimensional zeolites; we observed dramatically better coke tolerance over ZSM-12 (one dimensional) than USY (three dimensional). It was observed that samples synthesized with low Si/Al ratios resulted in higher activity and selectivity to the desired products. This was mainly because of the high hydrogen transfer (HT) capability of the low Si/Al samples. However, the dealumination procedure used strongly affected the catalyst performance; samples dealuminated with ammonium hexafluorosilicate were significantly less active and selective to TMPs than samples either dealuminated with HCl or synthesized directly. This was primarily because of the ability of the latter dealuminating agent to remove surface aluminum as well as partial pore blocking by the silicate salts deposited.** © 2002 Elsevier Science (USA)

*Key Words:* **alkylation; zeolites; dimensionality; pore structure; acidity; dealumination.**

## INTRODUCTION

The low-temperature alkylation of i-butane with light olefins for the production of high-octane compounds is of increasing importance for the refining industry. In particular, the 1990 Clean Air Act Amendments severely limited the amount of aromatics allowed in the gasoline pool, thus decreasing the net octane number—this can be made up for by using clean-burning alkylate compounds. Also, environmental concerns over MTBE and its expected removal from the gasoline pool will require further increases in clean-burning, high-octane blending components, of which alkylate is a prime choice. Traditionally, liquid acids such as HF and $H_2SO_4$ have been used in industry to catalyze alkylation reactions. However, several drawbacks and concerns related to the environment accompany their use, which necessitate their immediate replacement. The use of immobilized acids on solid supports or superacids such as sulfated zirconia has been investigated, but gradual leaching of the acid(s) results in catalyst deactivation and contamination of the product stream with less desirable products.

Acid zeolites are good candidates for this reaction but they possess relatively low acid site densities and low activity at the decreased temperatures where operation commonly takes place. Moreover, quick deactivation occurs for several zeolite-based systems, thus rendering the catalyst of limited use. Several zeolites have been tested in the past for the alkylation of i-butane with light olefins at low temperatures. Y faujasite was studied by several groups in its ultrastable (USY) form (1–5), or loaded with rare earth metals such as lanthanum (6). It was found that Y faujasite deactivates relatively fast regardless of the operating conditions. Corma and co-workers (1) concluded that

[1] To whom correspondence should be addressed. Fax: (513) 556-3473. E-mail: Panagiotis.Smirniotis@uc.edu.



0021-9517/02 $35.00

product selectivity and activity depend strongly on the strength distribution of Brønsted acid sites, on the extent of hydrogen transfer reactions, and on the concentration of reactants in the pores. It was also discovered that the dominant type of reactions follow the sequence cracking, alkylation, and finally oligomerization with respect to time due to the gradual deactivation of the acid sites. Others (2) found by considering intracrystalline mass transfer resistances that Y-type zeolites suffer from relatively low rates of hydride transfer reactions in regard to olefin addition. Beta has been tested as well and was found to be a very promising catalyst (7–12). Similar to USY, beta passes through successive changes in activity; cracking, alkylation, and oligomerization progressively dominate with time on stream. A comparison of beta with USY shows that the former results in relatively higher selectivities for alkylate. A study of beta samples with various Si/Al ratios revealed that the alkylate yield during the catalyst lifetime is proportional to the number of Brønsted acid sites (12). Moreover, they concluded that samples with low external surface area suffer from intracrystalline diffusional limitations. Large-pore zeolites of the ZSM-family combined with Lewis acid sites (13, 14) and molecular sieves such as MCM-36, MCM-49 (15), and MCM-41 (16) were studied as well.

In the present study we investigated the performance of selected three-, two-, and one-dimensional, large-pore zeolites with various Si/Al ratios for the low-temperature liquid-phase alkylation of *i*-butane with 2-butene. The WHSV of the olefin was kept very low in comparison with that of other studies (1) to allow us to better monitor the changes in product selectivity without oligomerization. The main goal was to relate time-on-stream activity and product selectivity not only with acidity characteristics of the samples but also with the zeolite dimensionality and pore architecture as well. In contrast to the common belief that three-dimensional zeolites are less suspectible to pore plugging than one-dimensional zeolites (17), we observed better coke tolerance over ZSM-12 (one dimensional) than USY (three dimensional). The present work, which is based on a polymolecular reaction, extends our earlier findings (18, 19) for monomolecular reactions; the specific pore geometry of zeolite catalysts greatly affects the observed time-on-stream stability and product selectivities for a given reaction and thus must be taken into account when selecting a particular catalyst.

## EXPERIMENTAL

### *Catalyst Preparation*

The zeolites used in this study include the three-dimensional USY (pore size of 7.4 Å and supercages of 13 Å) and beta (pore sizes of $7.3 \times 6.5$ and $5.6 \times 5.6$ Å), the two-dimensional mordenite (12-membered ring pores of $6.5 \times 7.0$ Å connected by twisted eight-membered ring pores of size $2.6 \times 5.7$ Å), and the one-dimensional LTL (7.1-Å pore size with periodic expansions of 12.6 Å) and ZSM-12 (straight, noninterpenetrating channels of size $5.6 \times 6.1$ Å). The USY samples were obtained from Zeolyst International (formerly the PQ Corp.) and were used without further modifications. The parent mordenite and L zeolite samples were obtained from UOP. Beta was synthesized from the corresponding aluminosilicate gel in our lab. Details of the synthesis have been described elsewhere (20). ZSM-12 was synthesized hydrothermally following the procedure described in detail by Gopal *et al.* (21). The synthesized zeolites were calcined in air at 520°C for 4 h to remove the occluded template. The ammonium form of each zeolite was obtained by performing a cation exchange of the charge-balancing alkali metal with $NH_4^+$. This procedure involved heating the sample in a 2.0 M $NH_4Cl$ solution at 90°C for 6 h under reflux.

Dealumination of selected zeolites was performed by acid leaching with HCl, steam treatment, or treatment with ammonium hexafluorosilicate (AHF), or by a combination of treatments. The procedure for dealumination with HCl involved the addition of 2 g of the ammonium form of the zeolite to a 950-ml HCl acid solution (1 N) at 85°C under reflux conditions followed by stirring for 4 h. Steam treatment was performed at 620°C for 4 h. The ammonium hexafluorosilicate procedure was as follows: 800 ml of water, 7 g of ammonium acetate, and 2 g of the ammonium form of the zeolite were added to a 1-liter, three-necked flask, followed by dropwise addition of an aqueous solution of $(NH_4)_2SiF_6$ and heating at 85°C under reflux conditions for 24 h in the case of mordenite and for 2 h in the case of L zeolite. Table 1 lists the zeolites and dealuminating procedures used.

### *Catalyst Characterization*

From $NH_3$-stepwise temperature-programmed desorption (STPD), the numbers of acid sites were obtained (Table 1). The $NH_3$-STPD experiments were a modification of the traditional temperature-programmed desorption procedure. The constant heating rate used in the conventional procedure was replaced with an optimized stepwise heating profile. The exact procedure is described elsewhere (22, 23).

The Si/Al ratios of the zeolites were determined by measuring the bulk silicon and aluminum content. These measurements were performed using inductively coupled plasma (ICP) emission spectroscopy. It should be noted that these measurements result in the bulk Si/Al ratio and are unable to differentiate between framework and nonframework aluminum species. The textural properties of zeolites were determined from the nitrogen isotherms at 77 K measured in a Micromeritics ASAP 2010 apparatus. All samples were degassed with He for 2 h at 200°C prior to measurement. XRD was employed for the identification of the synthesized zeolite phases and quantification of the

**TABLE 1**

**Properties of the Large-Pore Zeolites Used in the Present Study**

| Zeolite and pore structure | Pore structure schematic | Zeolite samples | Si/Al (bulk) | Dealumination method | No. Acid sites (mmol/g) | % Crystallinity | Mean diameter (μm) |
|---|---|---|---|---|---|---|---|
| USY, 3-D, 7.4 Å | 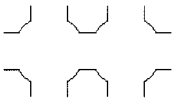 | Y-2.5 | 2.5[a] | As received | 2.21 | 100 | 2.1 |
| | | Y-6 | 6[a] | As received | 0.81 | 83 | — |
| | | Y-30 | 30[a] | As received | 0.40 | 72 | — |
| | | Y-40 | 40[a] | As received | 0.21 | 61 | — |
| Mordenite, 2-D, 7 × 6.5 and 5.7 × 2.6 Å |  | M-10 | 10[b] | As received | 1.31 | 100 | 2.5 |
| | | M-13 | 13[b] | 1.8 g AHF | 1.18 | 77 | — |
| | | M-35 | 35[b] | 1.0 N HCI | 0.51 | 109 | — |
| Beta, 3-D, 7.3 × 6.5 and 5.6 × 5.6 Å | 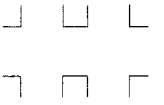 | B-15 | 15[b] | Synthesized | 0.69 | 100 | 1.5 |
| | | B-26 | 26[b] | 2.0 g AHF[c] | 0.53 | 100 | — |
| | | B-30 | 30[b] | Synthesized | 0.49 | 100 | — |
| LTL, 1-D, 7.1 Å | 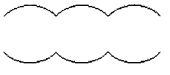 | L-3.5 | 3.5[b] | As received | 1.16 | 100 | 0.9 |
| | | L-6.5 | 6.5[b] | St[d]/1.4 g AHF | 0.85 | 71 | — |
| | | L-20 | 20[b] | 2 × (St/1.4 g AHF) | 0.70 | 60 | — |
| ZSM-12, 1-D, 5.6 × 6.1 Å | 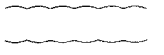 | Z-38 | 38[b] | Synthesized | 0.36 | 100 | 1.2 |
| | | Z-45 | 45[b] | Synthesized | 0.27 | 100 | — |
| | | Z-58 | 58[b] | Synthesized | 0.25 | 100 | — |

[a] Reported by company.
[b] Measured by ICP.
[c] AHF refers to ammonium hexafluorosilicate.
[d] St indicates steam treatment.

crystallinities of dealuminated zeolite. The XRD patterns were collected with a Siemens (D500) powder X-ray diffractometer using Cu$K\alpha$ radiation (wavelength, 1.5406 Å). The estimation of crystallinity was carried out based on the heights of the main crystallographic peaks of each zeolite.

X-ray photoelectron spectroscopy was performed to determine the Al and Si concentrations at the surface of selected samples. The XPS measurements were conducted on a Perkin–Elmer Model 5300 X-ray photoelectron spectrometer with a Mg$K\alpha$ radiation source at 300 W. The pass energies used for the survey and high-resolution modes were 89.45 and 35.75 eV, respectively. The binding energies and the total integrated peak areas of the Al 2p, Si 2p, and O 1s were used to calculate surface Si/Al ratios.

The amount of carbonaceous material remaining in the zeolite after reaction was measured by thermogravimetric analysis (Perkin–Elmer TGA7). The catalyst was kept at 100°C for 2 h to remove any volatile compounds to allow the weight to become constant. The carbonaceous material on the catalyst was then combusted at a temperature increase rate of 5°C/min to 550°C under a flow of oxygen (20 $cm^3$/min) and the weight change of the catalyst during oxidation was followed. After the oxidation step, the catalyst was cooled to 100°C and the difference in weight was measured. The ratio of this weight difference to the weight of the catalyst yielded the weight percent of carbonaceous material in the catalyst.

The diffusivity of hydrocarbon was measured by thermogravimetric analysis (Perkin–Elmer TGA7) during the adsorption of probe materials. This study was performed in order to explain the product selectivity based on the diffusivity limitation related to the pore structure of zeolites. A series of TMP isomers with increasing kinetic diameters ranging from 5.6 (2,3,4-TMP) to 7.0 Å (2,2,4-TMP) was used to determine the molecular transport inside pore. The ratio of diffusivity coefficients was estimated by applying Fick's law (24):

$$\frac{M_t}{M_\infty} = \frac{6}{r\sqrt{\pi}}\sqrt{Dt}.$$

For calculation of the ratio of the diffusion coefficient the slope of the linear part of the plot $M_t/M_\infty$ vs $t^{1/2}$ ($0.3 < M_t/M_\infty < 0.7$) was used.

The size of zeolite crystallites was determined with a laser scattering particle size analyzer (Malvern Mastersizer S series). For this experiment, the wet method was used as the medium for dispersion of the zeolite. The solution was ultrasonicated for 30 min in order to break down the flocculates before the run was carried out. All samples were run twice to ensure the accuracy of the measurements.

*Catalytic Studies*

A high-pressure, low-temperature reactor system has been developed for the alkylation of isobutane with 2-butene. The catalyst (typically 1 g) was loaded in a 1/2-in. stainless-steel vertical tube containing a 1/8-in.-diameter thermocouple. Dead volume in this reactor tube was

decreased using glass beads (Kimble Glass Inc., 3-mm diameter). Prior to each reaction run, the catalyst was pretreated *in situ* under a flow of nitrogen at 500°C for 2 h followed by a flow of oxygen at 450°C for 2 h. The reactor was then pressurized with nitrogen; pressure regulation was achieved using a Tescom backpressure regulator. For mechanistic studies which require real alkylation conditions, very-low-olefin feed stream (i/o molar ratio of 1000, olefin WHSV of 0.01 $h^{-1}$) was pumped to the system to suppress oligomerization. The GC analysis of the products was carried out at a catalyst time on stream of 5 min. For the remaining studies, pure isobutane was introduced into the system by ISCO syringe pump (model 100 DM) and then a mixture of isobutane and 2-butene (i/o molar ratio of 98) was pumped into the system using another ISCO syringe pump (model 500D) to prevent a chromatographic sorption/reaction of 2-butene on the zeolites. A weight hourly space velocity (WHSV) of 0.1 $h^{-1}$ (based on the olefin) was used for every run. A furnace was used to maintain a temperature of 80°C during the reaction. The reactor effluent was sent to a 16-port sampling valve (Vici-Valco) and product samples were taken periodically and stored in heated loops. These samples were analyzed using a gas chromatograph (Hewlett–Packard, 6890). The GC column used for separation was a Supelco Petrocol DH capillary column (50 m × 0.1 mm × 0.1 μm). Initial qualitative identifications of the products were accomplished with the help of a gas chromatograph (Hewlett–Packard, 5890 Series II) equipped with a mass spectrometer (Hewlett–Packard, 5972 Series II).

**TABLE 2**

**Initial Product Selectivity of Individual Compounds Obtained over Parent Samples**

| Sample | Y-2.5 | M-10 | B-15 | L-3.5 | Z-38 |
|---|---|---|---|---|---|
| 2-Butene conversion (wt%) | 100.00 | 100.00 | 100.00 | 100.00 | 100.00 |
| C5 (wt%) | 10.48 | 5.78 | 9.88 | 5.77 | 12.25 |
| C6 (wt%) | 5.99 | 4.40 | 4.46 | 2.98 | 5.70 |
| C7 (wt%) | 9.62 | 5.04 | 11.13 | 7.69 | 12.44 |
| C8 (wt%) | 69.47 | 80.05 | 70.23 | 82.88 | 64.62 |
| C9+ (wt%) | 4.43 | 4.74 | 4.30 | 0.68 | 4.99 |
| Distribution of C8 (wt%) | | | | | |
| TMPs | 59.97 | 62.39 | 57.43 | 75.30 | 49.33 |
| 2,2,3-TMP | 3.53 | 0.44 | 0.55 | 3.24 | 0.43 |
| 2,2,4-TMP | 18.22 | 32.04 | 34.27 | 23.22 | 27.08 |
| 2,3,3-TMP | 19.65 | 9.01 | 7.60 | 14.85 | 6.24 |
| 2,3,4-TMP | 18.57 | 20.91 | 15.00 | 34.00 | 15.58 |
| DMHs | 9.18 | 17.65 | 12.48 | 7.21 | 15.30 |
| 2,2-DMH | 0.00 | 0.11 | 0.00 | 0.00 | 0.00 |
| 2,3-DMH | 3.85 | 6.43 | 4.84 | 3.68 | 6.84 |
| 2,4-DMH | 2.80 | 5.90 | 3.86 | 1.75 | 4.16 |
| 2,5-DMH | 1.13 | 4.16 | 3.40 | 0.64 | 3.99 |
| 3,3-DMH | 0.00 | 0.15 | 0.00 | 0.00 | 0.00 |
| 3,4-DMH | 1.40 | 1.60 | 0.68 | 1.14 | 0.79 |
| MHept | 0.00 | 0.00 | 0.00 | 0.00 | 0.00 |
| 2-MH | 0.00 | 0.00 | 0.00 | 0.00 | 0.00 |
| 3-MH | 0.00 | 0.00 | 0.00 | 0.00 | 0.00 |
| 4-MH | 0.00 | 0.00 | 0.00 | 0.00 | 0.00 |
| 3-E,2-M pentane | 0.32 | 0.00 | 0.32 | 0.36 | 0.00 |
| C8 olefin | 0.00 | 0.00 | 0.00 | 0.00 | 0.00 |

*Note.* Reactions were performed at 80°C and 300 psi ($WHSV_{olefin}$ = 0.01 $h^{-1}$, $i/o_{molar}$ ratios = 1000). Time on stream, 5 min.

## RESULTS AND DISCUSSION

### *Mechanism Study*

The mechanism of alkylation has been studied intensively in the past (2, 17, 25). However, it is hard to explain that the entire path occurred in the alkylation due to its complicated chain mechanism. In order to avoid the undersirable oligomerization reaction leading to complicated reaction pathways, the alkylation was performed under mild deactivating conditions (i/o molar ratio of 1000, olefin WHSV of 0.01 $h^{-1}$). The parent zeolites were employed to avoid any effects due to structural changes caused by dealumination. The results obtained within 5 min on stream showed 100% olefin conversion and less than 5 wt% $C9^+$ products (see Table 2). Thus, we were able to investigate the product selectivity under real alkylation conditions.

In the main sequence, a *sec*-butyl carbenium ion is formed by the protonation of 2-butene over an acid site (Reaction 1). This cation then undergoes a hydride transfer to isobutane to form a *tert*-butyl carbenium ion. Thereafter, the *tert*-butyl carbenium ion reacts with another 2-butene molecule to form trimethylpentane carbocations. Another hydride transfer is necessary to form alkylation products, trimethylpentanes (TMPs), from TMP carbocations. Hence, two hydride transfers are required to complete the alkylation (Reaction 2):

$$sec\text{-}C_4^= + H^+ \rightarrow sec\text{-}C_4^+, \quad [1]$$

$$sec\text{-}C_4^+ + \text{i-}C_4 \xrightarrow{HT} n\text{-}C_4 + \text{i-}C_4^+ \xrightarrow{2\text{-}C_4^=} 2,2,3\text{-}TMP^+ \xrightarrow{\text{isomerization}} TMPs^+ \xrightarrow{HT} TMPs. \quad [2]$$

By examining the distribution of trimethylpentanes, one can observe that 2,2,3-TMP, the primary product of alkylation, was at relatively low concentrations. This was attributed to the fast isomerization of its transition state on the acid sites (1). The rearrangement of the $2,2,3\text{-}TMP^+$ carbocation into the other $TMP^+$ isomer occurs rapidly before the primary carbocation desorbs from the acid sites.

For the selectivity of other TMPs, one can observe various distributions over each zeolite, as illustrated in Table 2. This can be explained with regard to the kinetic diameter of these isomers. The formation of the bulkiest isomers (2,2,4- and 2,2,3-TMP) goes through a transition state that presents more steric hindrance than occurs for smaller isomers (2,3,3- and 2,3,4-TMP). Indeed, Corma and Martinez (17) have shown that the (2,2,4 + 2,2,3)/(2,3,4 + 2,3,3) ratio can be directly related to the selectivity of zeolites; larger pore size zeolites yield higher levels of this ratio. Unexpectedly,

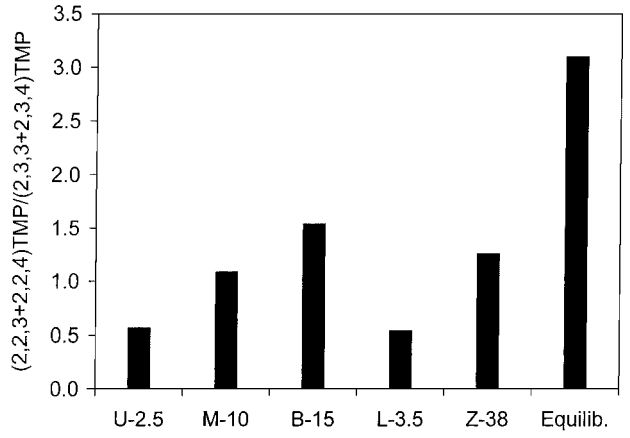


**FIG. 1.** Ratio of (2,2,4 + 2,2,3)/(2,3,4 + 2,3,3)-TMPs for selected zeolites. Reactions were performed at 80°C and 300 psi ($WHSV_{olefin}$ = 0.01 $h^{-1}$, $i/o_{molar}$ = 1000).

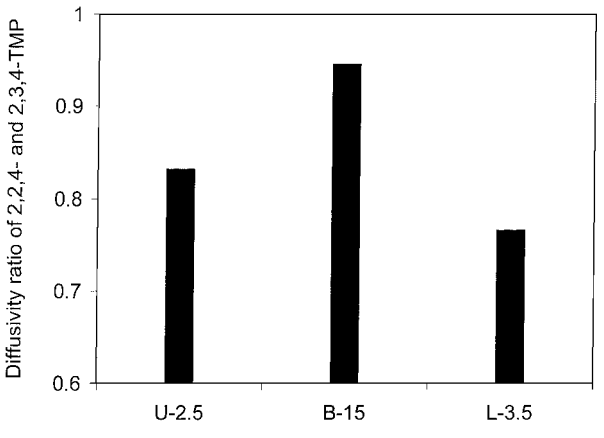


**FIG. 2.** Diffusivity ratio of 2,2,4- and 2,3,4-TMPs for selected zeolites.

we observed that this ratio is more dependent on pore shape than size (Fig. 1). Beta and ZSM-12 showed higher values than did USY and LTL. This is believed to be a result of the specific pore architecture of beta and ZSM-12; the lack of expansions in these zeolites that are significantly larger than the pore openings prevent to some extent steric hindrance of the TMP isomers. For USY and LTL samples with large supercages, the selectivities of 2,2,4-TMP are higher than those of 2,2,3-TMP but not as high as one would expect based on the thermodynamic equilibrium. Evidently, the relatively large size of the 2,2,3- and 2,2,4-TMP transition-state intermediates disfavors their production even inside the large pores of USY and LTL. It is worth noting that the selectivities of 2,3,3- and 2,3,4-TMP are surprisingly high if one considers that it is not favored thermodynamically. Evidently, the relatively high concentrations of them are attributed to the fact that its transition-state intermediate is the smallest and thus it can easily diffuse out of the pores.

The diffusivity ratio of 2,2,4-TMP (7.0 Å) and 2,3,4-TMP (5.6 Å) was obtained to support the idea that the diffusional limitations imposed by the zeolite structure play a determining role in the final product distribution. The diffusivity ratio of probe molecules over USY, beta, and LTL is shown in Fig. 2. The selected zeolites possess comparable pore size (over 7.0 Å) where the probe molecules can access inside. It is observed that for beta with favorable pore structure (no expansions), the diffusivity ratio 2,2,4-TMP to 2,3,4-TMP was close to one (0.95). For other zeolites which possess wide channel intersections or supercages being connected with regions of significantly smaller diameter, the ratio was less than one. The difference in the ratio of diffusivity was reflected in the product distribution of the TMP isomers. Moreover, the mean particle diameter was measured to investigate the effect of crystal size on the product distributions. It is observed that the crystal size of samples hardly affected the determination of TMP distributions (see Table 1).

The *sec*-butyl carbenium ion may react with another 2-butene molecule to form 3,4-dimethylhexane (DMH) cations. This $DMHs^+$ may then undergo any number of hydride or methyl shifts, thus leading to all possible DMH isomers (Reaction 3):

$$sec\text{-}C_4^+ \xrightarrow{2\text{-}C_4^=} 3,4\text{-}DMHs^+ \xrightarrow{\text{isomerization}} DMHs^+ \xrightarrow{HT} DMHs. \quad [3]$$

The selectivity of DMHs was also affected by pore structure. The ratio of isomers to primary product from dimerization of two 2-butene (2,5-,2,4-,2,3-DMH/3,4-DMH) is presented in Fig. 3. Beta and ZSM-12, which possess similar pore structure, showed high values than others. Other samples with comparable pore structures, USY, and LTL showed lower values. In addition, 2,2-DMH can be produced by another reaction path involving 1-butene. However, it was not detected in our reaction, which may be due

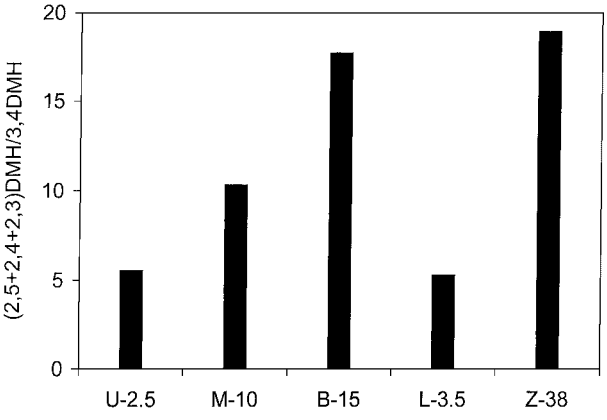


**FIG. 3.** Ratio of (2,5 + 2,4 + 2,3)/3,4-DMHs for selected zeolites. Reactions were performed at 80°C and 300 psi ($WHSV_{olefin}$ = 0.01 $h^{-1}$, $i/o_{molar}$ = 1000).

to the fact that only 1% 1-butene exists in equilibrium conditions (25).

Methyl heptane ($MHs^+$) isomers may be formed by condensation of 1-butene with 2-butene (Reaction 4) (as explained above, no products were obtained due to the reaction with 1-butene):

$$sec\text{-}C_4^+ \xrightarrow{1\text{-}C_4^=} MPs^+ \xrightarrow{HT} MHs, \quad [4]$$

$$i\text{-}C_8^+ \xrightarrow{C_4^=} i\text{-}C_{12}^+ \xrightarrow{C_4^=} i\text{-}C_{16}^+. \quad [5]$$

At the initial stage (time on stream of 5 min), most of C5–C7 products were yielded by cracking activity from heavy products formed by polymerization (C12 and C16, Reaction 5) (26). Based on the accepted cracking mechanism (27), several types of β-scissions existed, for example types A, B1, B2, C, D. Considering the reaction temperature for alkylation (80°C), type A β-scission (from tertiary to tertiary carbenium ion) should occur preferentially. As major products from C5–C7 (see Table 3), we observed 2-methyl butane (C5), 2,3-dimethyl butane (C6), and 2,3- and 2,4-dimethyl pentane (C7). These hydrocarbons were formed by type A β-scissions, as illustrated in Fig. 4. The olefins (less than C9) formed by cracking activity could not be detected; they might be involved in the alkylation reaction the same as other olefin reactants. Low amounts of heavy hydrocarbons were detected at the initial stage. The range of these was C9–C11, which could be formed by cracking from $C_{16}H_{33}^+$ cations (see Fig. 4). This indicates that the oligomerization activity producing heaver materials (over C12) was very limited in this stage due to a highly active catalyst.

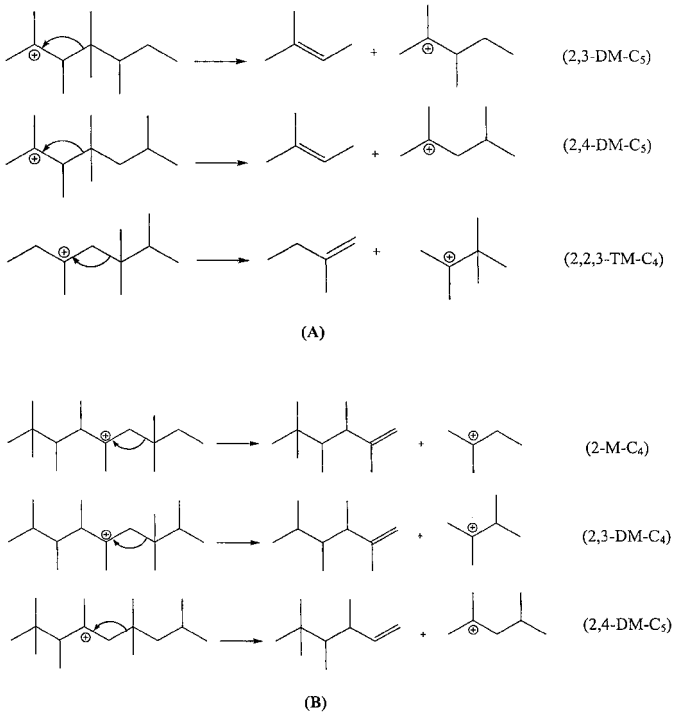


**FIG. 4.** The mechanism of major cracking products (C5–C7). (A) Type A β-scissions starting from selected $C_{12}H_{25}^+$ cations with five branchings. (B) Type A β-scissions starting from selected $C_{16}H_{33}^+$ cations with seven branchings.

**TABLE 3**

**Initial Selectivity of Individual Compounds without C8 Products Obtained over Parent Samples**

| Sample | Y-2.5 | M-10 | B-15 | L-3.5 | Z-38 |
|---|---|---|---|---|---|
| 2-Butene conversion (wt%) | 100.00 | 100.00 | 100.00 | 100.00 | 100.00 |
| Distribution of C5 (wt%) | 10.48 | 5.78 | 9.88 | 5.77 | 12.25 |
| 2-Methyl butane | 10.48 | 5.78 | 9.88 | 5.77 | 12.25 |
| *n*-Pentane | 0.00 | 0.00 | 0.00 | 0.00 | 0.00 |
| Distribution of C6 (wt%) | 5.99 | 4.40 | 4.46 | 2.98 | 5.70 |
| 2,2-DM butane | 0.00 | 0.00 | 0.00 | 0.00 | 0.00 |
| 2,3-DM butane | 4.27 | 1.91 | 3.29 | 2.03 | 4.48 |
| 2-M pentane | 0.88 | 1.16 | 0.75 | 0.47 | 0.77 |
| 3-M pentane | 0.84 | 1.33 | 0.42 | 0.48 | 0.45 |
| *n*-Hexane | 0.00 | 0.00 | 0.00 | 0.00 | 0.00 |
| Distribution of C7 (wt%) | 9.62 | 5.04 | 11.13 | 7.69 | 12.44 |
| 2,2,3-TM butane | 0.23 | 0.45 | 0.21 | 0.13 | 0.28 |
| 2,2-DM pentane | 0.00 | 0.00 | 0.00 | 0.00 | 0.00 |
| 2,3-DM pentane | 4.60 | 2.03 | 4.27 | 4.39 | 5.08 |
| 2,4-DM pentane | 4.20 | 1.22 | 6.08 | 2.88 | 6.53 |
| 3,3-DM pentane | 0.00 | 0.00 | 0.00 | 0.00 | 0.00 |
| 2-M hexane | 0.26 | 0.67 | 0.42 | 0.12 | 0.37 |
| 3-M hexane | 0.33 | 0.67 | 0.15 | 0.17 | 0.18 |
| 3-Ethyl pentane | 0.00 | 0.00 | 0.00 | 0.00 | 0.00 |
| *n*-Heptane | 0.00 | 0.00 | 0.00 | 0.00 | 0.00 |
| C9 (wt%) | 3.04 | 3.09 | 2.45 | 0.46 | 2.39 |
| C10 (wt%) | 1.16 | 0.69 | 1.20 | 0.11 | 1.23 |
| C11 (wt%) | 0.23 | 0.96 | 0.65 | 0.11 | 1.37 |

*Note.* Reactions were performed at 80°C and 300 psi ($WHSV_{olefin}$ = 0.01 $h^{-1}$, $i/o_{molar}$ ratios = 1000). Time on stream, 5 min.

The oligomerization of butene may also occur with the decrease in the hydrogen transfer activity, thus producing the heavy end products. A dodecyl cation is formed by oligomerization of butene with an octyl cation. Similarly, a hexadecyl cation is produced by butene addition to a dodecyl cation. Most of olefins are formed in these reaction pathways. Hydrocarbons above C16, however, are unable to diffuse out of the zeolite pore structure and are not obtained as products. These compounds may lead to catalyst deactivation by remaining either adsorbed on the acid site (acid site poisoning) or within the pores as carbonaceous materials (pore plugging).

*USY*

USY in the acidic or modified form (metals such as Ce, La) has been tested extensively by numerous groups as an alkylation catalyst. The pore openings of Y faujasite (7.4 Å) provide sufficient space to allow the existence of the relatively bulky transition-state intermediates involved in the synthesis of multibranched paraffins or alkylaromatics. Moreover, the relatively high aluminium density of USY

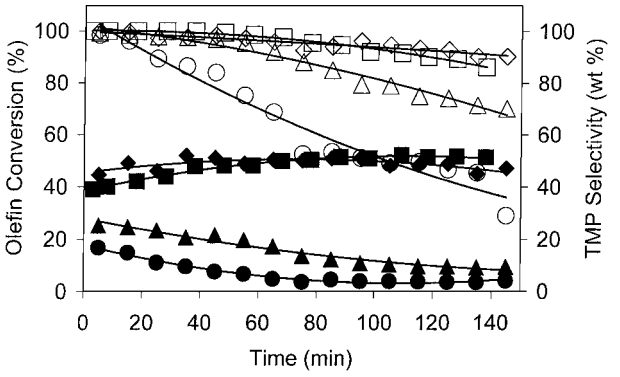


**FIG. 5.** Olefin conversion (open symbols) and TMP selectivity (closed symbols) for Y-2.5 (◇, ◆), Y-6.0 (□, ■), Y-30 (△, ▲), and Y-40 (○, ●). Reactions were performed at 80°C and 300 psi ($WHSV_{olefin} = 0.1\ h^{-1}$, $i/o_{molar} = 98$).

offers numerous acid sites or sites that act as ligands for the addition of metal(s). This explains the wide use of faujasites in refining and chemical industries despite the fact that their pore structure, namely regions of high space (supercages of about 12 Å) being connected with regions of significantly smaller diameter (7.4 Å), renders the catalyst susceptible to coking. This coking behavior is a strong indication that high dimensionality does not always guarantee stability. Based on both our previous and present work we believe that the relation of the size of the zeolite aperture to that of the supercage/channel intersection plays a very important role in the catalyst activity; when the channel intersection is comparable with the aperture, improved time stability can be achieved.

The 2-butene conversion as a function of time on stream for USYs of different Si/Al ratios is presented in Fig. 5. One can observe a monotonic increase in deactivation with an increase in the bulk Si/Al ratio. This increase becomes more noticeable for the samples with the lowest aluminum content, namely samples with Si/Al of 30 and 40. This deactivation trend with respect to Si/Al at the present operating conditions (80°C and liquid phase) is in contrast with the deactivation behavior of zeolites observed at elevated temperatures, where the tolerance to coking improves with the decrease in acid site density. At low temperatures (below 80°C), such as those employed in the present study, where the products can easily remain on the surface, the only mechanism for preserving acid sites that are free of carbonaceous compounds (unsaturated hydrocarbons) is to drive adsorbed compounds away from the surface. This is achieved via hydrogen transfer reactions (HTR), which involve the transfer of hydrogen atoms from hydrocarbons of the bulk phase to surface intermediates. This leads to desorption of the latter species from the surface.

It was observed that the cracking activity of low Si/Al zeolite (Y-2.5) was quite stable for the entire time on stream (not shown) due to the very large number of acid sites. In contrast, the amount of cracked products obtained over the high Si/Al zeolite (Y-40) strongly decreased within a short time on stream. On the other hand, the formation of olefins rapidly increased at the same time on stream. It is shown that the cracking activity increases when increasing the Al concentration of a zeolite. However, the slightly dealuminated zeolite (Y-6) produced higher amounts of cracking products than either the parent zeolite or the other dealuminated samples (Table 4). It is well-known that the strength of acidity increases by mild dealumination, indicating that this reaction occurs on strong acid sites.

The selectivities of the trimethylpentane isomers which are the desirable products of this reaction are presented as

**TABLE 4**

**Initial Product Selectivity of Individual Compounds Obtained over USY Samples**

| Samples | Y-2.5 | Y-6 | Y-30 | Y-40 |
|---|---|---|---|---|
| 2-Butene conversion (wt%) | 100.00 | 100.00 | 99.44 | 98.51 |
| *n*-Butane (wt%) | 2.97 | 2.95 | 0.81 | 0.53 |
| Distribution of C5 (wt%) | 13.43 | 23.34 | 15.99 | 13.21 |
| 2-Methyl butane | 13.43 | 23.34 | 15.99 | 13.21 |
| *n*-Pentane | 0.00 | 0.00 | 0.00 | 0.00 |
| Distribution of C6 (wt%) | 6.46 | 9.99 | 8.13 | 7.51 |
| 2,2-DM butane | 0.00 | 0.00 | 0.00 | 0.00 |
| 2,3-DM butane | 4.47 | 6.63 | 4.68 | 3.55 |
| 2-M pentane | 0.90 | 1.91 | 1.74 | 2.08 |
| 3-M pentane | 1.10 | 1.45 | 1.71 | 1.88 |
| *n*-Hexane | 0.00 | 0.00 | 0.00 | 0.00 |
| Distribution of C7 (wt%) | 8.41 | 10.27 | 8.38 | 7.48 |
| 2,2,3-TM butane | 0.33 | 0.30 | 0.40 | 0.33 |
| 2,2-DM pentane | 0.00 | 0.00 | 0.00 | 0.00 |
| 2,3-DM pentane | 3.68 | 3.48 | 4.00 | 3.58 |
| 2,4-DM pentane | 3.78 | 5.52 | 2.71 | 1.91 |
| 3,3-DM pentane | 0.00 | 0.00 | 0.00 | 0.00 |
| 2-M hexane | 0.25 | 0.49 | 0.44 | 0.56 |
| 3-M hexane | 0.37 | 0.49 | 0.83 | 1.10 |
| 3-Ethyl pentane | 0.00 | 0.00 | 0.00 | 0.00 |
| *n*-Heptane | 0.00 | 0.00 | 0.00 | 0.00 |
| Distribution of C8 (wt%) | 54.66 | 48.32 | 43.64 | 39.98 |
| 2,2,3-TMP | 2.21 | 3.11 | 1.00 | 0.62 |
| 2,2,4-TMP | 10.66 | 12.33 | 8.96 | 6.26 |
| 2,3,3-TMP | 14.40 | 11.57 | 5.80 | 3.69 |
| 2,3,4-TMP | 17.28 | 12.05 | 9.48 | 6.24 |
| 2,2-DMH | 0.00 | 0.00 | 0.00 | 0.00 |
| 2,3-DMH | 3.86 | 3.03 | 8.76 | 11.71 |
| 2,4-DMH | 2.24 | 3.18 | 3.60 | 4.42 |
| 2,5-DMH | 0.90 | 1.69 | 1.57 | 1.59 |
| 3,3-DMH | 0.00 | 0.00 | 0.00 | 0.00 |
| 3,4-DMH | 2.71 | 1.10 | 4.04 | 4.99 |
| 2-MH | 0.00 | 0.00 | 0.00 | 0.00 |
| 3-MH | 0.00 | 0.00 | 0.00 | 0.00 |
| 4-MH | 0.00 | 0.00 | 0.00 | 0.00 |
| 3-E,2-M pentane | 0.38 | 0.26 | 0.42 | 0.47 |
| C5–C8 olefins | 0.52 | 0.34 | 0.73 | 1.18 |
| C9+ | 13.55 | 4.79 | 22.31 | 30.11 |

*Note.* Reactions were performed at 80°C and 300 psi ($WHSV_{olefin} = 0.1\ h^{-1}$, $i/o_{molar}$ ratios = 98). Time on stream: 5 min for all except Y-6, which was 3 min.

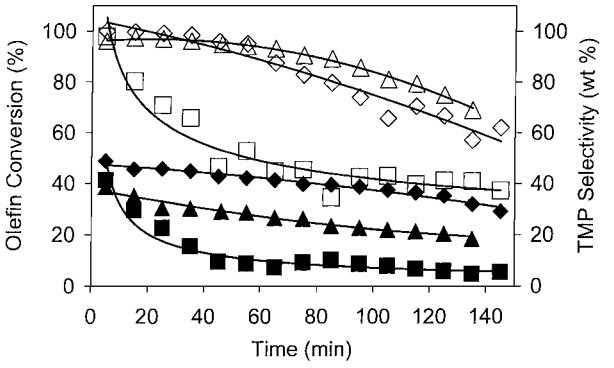


**FIG. 6.** Olefin conversion (open symbols) and TMP selectivity (closed symbols) for M-10 (◇, ◆), M-13 (□, ■), and M-35 (△, ▲). Reactions were performed at 80°C and 300 psi ($WHSV_{olefin} = 0.1\ h^{-1}$, $i/o_{molar} = 98$).

a function of time on stream (see Fig. 5). The concentration of trimethylpentanes (TMPs), which are the products of alkylation, acquired relatively high values. This indicates that the alkylation of i-butane with 2-butene takes place to a large extent; this was expected because of the high i-butane/2-butene ratio used in the feed. The selectivity to TMPs was higher for the samples with the lower Si/Al ratio and decreased with the aluminum content of the catalysts. This trend is related to the decrease in the hydrogen transfer capability that results in the decrease of t-$C4^+$ surface species, leading the formation of TMPs (Reaction 2). A similar trend can be found from the yield of *n*-butane at the initial stage from the alkylation experiments, as represented in Table 4. According to the well-known reaction mechanism (1), the protonation of the olefin followed by hydrogen transfer yields *n*-butane (Reaction 2). Hence, the amount of *n*-butane formed at the initial stage can be indicative of the hydrogen transfer activity of the catalyst.

*Mordenite*

The activity behavior of mordenite samples with various Si/Al ratios is presented in Fig. 6. One can observe an unexpected inversion in the olefin conversion profiles with respect to the Si/Al ratios. More specifically, the sample with Si/Al = 13 possessed high initial activity but dropped rapidly with time and finally acquired low values. This sample was dealuminated with $(NH_4)_2SiF_6$ (AHF) and contained slightly less aluminum than the parent sample (M-10) that was obtained from UOP. Of course, this decrease in the aluminum content cannot justify this steep decrease in activity. It is surprising to note that the M-35 sample preserved its activity to a much better extent than the M-13. This is in contrast with the general trend that the increase in Si/Al resulted in a monotonic increase in deactivation due to mainly the decrease in the hydrogen transfer capability. The explanation for this behavior is based partially on the surface Si/Al ratio of the samples in question. The M-10 sample possesses nearly uniform Al concentration throughout the

**TABLE 5**

**Physicochemical Properties of Selected Mordenite Samples**

| Sample name | Bulk Si/Al (ICP) | Surface Si/Al (XPS) | BET area ($m^2/g$) | Pore volume[a] ($cm^3/g$) |
|---|---|---|---|---|
| M-10 | 10 | 9.1 | 425 | 0.26 |
| M-13 | 13 | 18.7 | 267 | 0.17 |
| M-35 | 35 | 30.0 | 444 | 0.27 |

[a] Determined by Horvath–Kawazoe method.

sample. However, the dealumination procedures resulted in a concentration gradient, as shown in Table 5. Dealumination with AHF resulted in the preferential elimination of surface aluminum, thereby resulting in a surface Si/Al ratio that is greater than the bulk. Moreover, the fluorosilicate salt was trapped on the surface of M-13 during the dealumination. This would result in the formation of a silicate layer coating the crystals of M-13 and prohibiting access of the reagents to the pore (28). The decrease in pore volume and BET area by AHF dealumination supports well the above explanation (see Table 5).

Dealumination of mordenite with HCl resulted in a lower surface Si/Al ratio, indicating that the mechanism of HCl dealumination is a uniform migration of aluminum species from the inner core of the catalyst particle to the outer surface. The outer surface will therefore be enriched in aluminum, imparting the catalyst with increased activity. From the BET area and pore volume data (Table 5), it was observed that the M-35 sample possesses favorable properties to avoid diffusion limitation inside the pore (12).

It is well-known that most carbonaceous materials formed inside zeolite pores are adsorbed on spent acid sites. The amount of carbonaceous materials remaining inside the zeolites is illustrated in Fig. 7. We observed that the more-time-stable zeolites retained more carbonaceous material

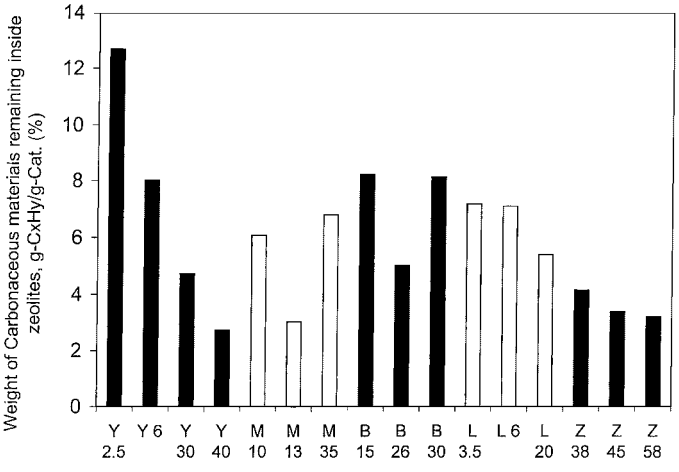


**FIG. 7.** Weight percent of carbonaceous materials remaining inside zeolites after reaction.

during the alkylation reaction, which is in agreement with earlier work (29). This is because in zeolites, the faster the pore mouth blocking by coke, the lower the use of the internal surface. Therefore, the lower amounts of carbonaceous materials were measured from the sample which deactivated rapidly. We believe that the number of accessible acid sites present in M-13 is limited because of pore plugging due to relatively fewer acid sites near the pore mouth and the silicate deposits inside the pores of the samples.

The trends of TMP selectivities over mordenite (Fig. 6) were comparable with that of olefin conversion. The initial selectivity for TMPs was relatively high, especially over the samples with the highest aluminum content. However, the gradual deactivation of the acid sites resulted in a decrease in the TMP selectivities with time on stream. The TMP selectivity over M-13 dropped rapidly with time on stream (see Fig. 6). This indicated that its relatively small pore size and volume by silicate deposits hardly allow the formation of TMPs, with relatively large kinetic diameter, inside the pore. Even though M-35 possessed a lower aluminum content, one observed relatively high amount of TMPs. Hence, zeolites with large amounts of acid sites could not guarantee the high TMP selectivity without favorable pore structure. The initial selectivity of 2,2,4-TMP over M-10 (Table 6) followed the values predicted by thermodynamics. However, the deactivation of the catalyst favored the formation of 2,3,4-TMP, which is the least bulky trimethylpentane isomer, and therefore fits easily inside the relatively smaller pores (6.5 × 7.0 Å) of mordenite.

*Beta*

The activity characteristics of beta are presented in Fig. 8 for various Si/Al ratios. The synthesized samples preserved their activity for the entire duration of the experimental run. The good stability of beta for acid-catalyzed reactions is primarily due to its pore architecture. Its 12-member ring pores form a three-dimensional network of channels. The diameters of the channel intersections are not significantly larger than the diameter of the apertures. A comparison of the time-on-stream characteristics of the USYs with beta of comparable Si/Al ratios shows that the latter zeolite was significantly better. This behavior cannot be attributed to differences in the acidity characteristics of these two zeolites since the concentration of acid sites is comparable for both zeolites (see Table 1). Moreover, since both zeolites are three dimensional the dimensionality of their pores cannot be responsible. Therefore, the specific pore characteristics of each zeolite are responsible for the different deactivation patterns observed. More specifically, the large supercages of USY favor to a higher extent the accumulation of unsaturated hydrocarbons inside the pores.

For activity of both beta zeolites (B-26 and B-30) with comparable acid density, one observed similarities with the mordenite samples, even though the dealuminated sample (B-26) possessed a higher number of acid sites, deactivating rapidly. This is attributed to the negative effects of AHF dealumination, as mentioned above. Thus, the structural properties of zeolites greatly affect the observed time-on-stream stability for this reaction.

For the lumped selectivities of TMPs over the beta zeolites, one observed similar behavior with mordenite, as presented in Fig. 8. In the case of the B-26 sample we observed a decrease in TMP selectivity with time. As explained for the M-13 sample, this can be attributed to the negative effect of dealumination with AHF. Other samples prepared by direct synthesis showed a constantly high amount of TMPs. However, the B-15 sample formed a slightly larger amount

**TABLE 6**

**Initial Product Selectivity of Individual Compounds Obtained over Mordenite Samples**

| Samples | M-10 | M-13 | M-35 |
|---|---|---|---|
| 2-Butene conversion (wt%) | 100.00 | 97.87 | 96.07 |
| *n*-Butane (wt%) | 2.12 | 1.31 | 1.24 |
| Distribution of C5 (wt%) | 5.76 | 5.23 | 12.88 |
| 2-Methyl butane | 5.76 | 5.23 | 12.88 |
| *n*-Pentane | 0.00 | 0.00 | 0.00 |
| Distribution of C6 (wt%) | 4.10 | 3.70 | 7.30 |
| 2,2-DM butane | 0.22 | 0.00 | 0.00 |
| 2,3-DM butane | 2.14 | 2.23 | 4.50 |
| 2-M pentane | 0.89 | 0.74 | 1.66 |
| 3-M pentane | 0.86 | 0.73 | 1.14 |
| *n*-Hexane | 0.00 | 0.00 | 0.00 |
| Distribution of C7 (wt%) | 3.49 | 4.04 | 5.33 |
| 2,2,3-TM butane | 0.14 | 0.00 | 0.13 |
| 2,2-DM pentane | 0.00 | 0.00 | 0.00 |
| 2,3-DM pentane | 1.29 | 1.65 | 2.22 |
| 2,4-DM pentane | 1.19 | 1.66 | 1.88 |
| 3,3-DM pentane | 0.09 | 0.00 | 0.00 |
| 2-M hexane | 0.45 | 0.39 | 0.71 |
| 3-M hexane | 0.33 | 0.34 | 0.39 |
| 3-Ethyl pentane | 0.00 | 0.00 | 0.00 |
| *n*-Heptane | 0.00 | 0.00 | 0.00 |
| Distribution of C8 (wt%) | 69.25 | 60.47 | 60.19 |
| 2,2,3-TMP | 0.57 | 0.36 | 0.13 |
| 2,2,4-TMP | 30.36 | 14.04 | 15.27 |
| 2,3,3-TMP | 7.29 | 5.05 | 2.42 |
| 2,3,4-TMP | 10.56 | 21.88 | 20.71 |
| 2,2-DMH | 0.32 | 0.00 | 0.00 |
| 2,3-DMH | 6.34 | 10.15 | 8.95 |
| 2,4-DMH | 6.95 | 4.63 | 6.25 |
| 2,5-DMH | 5.12 | 1.98 | 5.63 |
| 3,3-DMH | 0.70 | 0.39 | 0.22 |
| 3,4-DMH | 0.83 | 1.65 | 0.49 |
| 2-MH | 0.00 | 0.00 | 0.00 |
| 3-MH | 0.00 | 0.00 | 0.00 |
| 4-MH | 0.00 | 0.00 | 0.00 |
| 3-E,2-M pentane | 0.22 | 0.35 | 0.13 |
| C5–C8 olefins | 1.66 | 3.49 | 2.51 |
| C9+ | 13.61 | 21.76 | 10.55 |

*Note.* Reactions were performed at 80°C and 300 psi ($WHSV_{olefin}$ = 0.1 $h^{-1}$, $i/o_{molar}$ ratios = 98). Time on stream, 5 min.

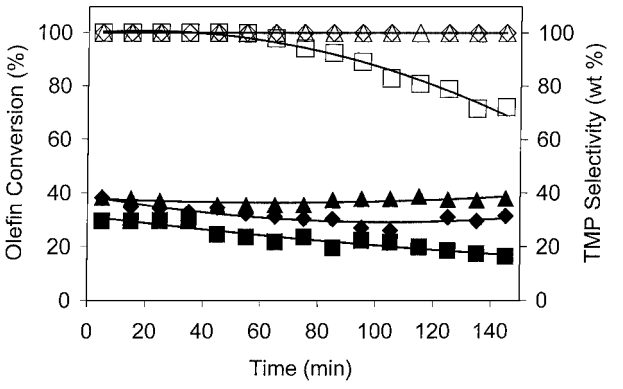


**FIG. 8.** Olefin conversion (open symbols) and TMP selectivity (closed symbols) for B-15 (◇, ◆), B-26 (□, ■), and B-30 (△, ▲). Reactions were performed at 80°C and 300 psi ($WHSV_{olefin} = 0.1\ h^{-1}$, $i/o_{molar} = 98$).

for TMPs than the B-30 sample due to higher acid sites, even though both samples possess comparable structural properties. The product selectivities of all beta zeolites (Table 7) show similarities regardless of Si/Al ratio. It should be noted that although the 2,2,4-TMP is the largest isomer, it is seen in the highest quantities. This is due to the specific pore architecture of beta, which allows the bulky isomer to diffuse out, as explained earlier section.

*LTL*

The activity of LTL with various Si/Al ratios is presented in Fig. 9. The activity of all samples decreased with time on stream. A monotonic increase in coking with Si/Al was observed. It is worth noting that the activity of the LTL sample with even the lowest Si/Al (L-3.5) decreased rapidly with time. This was not expected since the high aluminum concentration and thus high hydrogen transfer capability should keep the catalyst surface free of carbonaceous compounds. The one-dimensional pores of LTL consist of periodic expansions (12.6 Å) followed by regions of smaller diameter (7.1 Å) (30). This pore configuration renders the latter zeolite susceptible to coke. Indeed, the results obtained for both beta and ZSM-12 (see below) show that at low Si/Al the samples were very stable with time on stream. Evidently, the acidity characteristics of a zeolite (number and type of sites and strength distribution) that control the extent of acid-catalyzed reactions, including hydrogen tranfer reactions, are not sufficient to ensure stability. The specific pore architecture of a zeolite is an equally important factor in determining its time stability.

An inspection of the product selectivities of the LTL samples (Fig. 9) shows that the selectivities for TMPs were the highest among the octanes produced in comparison with all other zeolites. Moreover, the initial yields for C8 paraffins, which result from alkylation and oligomerization reactions, were the highest compared to all other zeolite tested. This is a very promising characteristic if high yields for alkylate are required. We believe that the possible reason for this

**TABLE 7**

**Initial Product Selectivity of Individual Compounds Obtained over Beta Samples**

| Samples | B-15 | B-26 | B-30 |
|---|---|---|---|
| 2-Butene conversion (wt%) | 100.00 | 100.00 | 100.00 |
| *n*-Butane (wt%) | 2.28 | 1.52 | 1.65 |
| Distribution of C5 (wt%) | 13.73 | 13.44 | 16.88 |
| 2-Methyl butane | 13.73 | 13.44 | 16.88 |
| *n*-Pentane | 0.00 | 0.00 | 0.00 |
| Distribution of C6 (wt%) | 7.01 | 7.17 | 8.54 |
| 2,2-DM butane | 0.00 | 0.00 | 0.00 |
| 2,3-DM butane | 4.84 | 4.99 | 5.32 |
| 2-M pentane | 1.42 | 1.47 | 1.93 |
| 3-M pentane | 0.74 | 0.71 | 1.29 |
| *n*-Hexane | 0.00 | 0.00 | 0.00 |
| Distribution of C7 (wt%) | 9.25 | 8.70 | 9.97 |
| 2,2,3-TM butane | 0.33 | 0.33 | 0.38 |
| 2,2-DM pentane | 0.00 | 0.00 | 0.00 |
| 2,3-DM pentane | 2.49 | 2.37 | 2.78 |
| 2,4-DM pentane | 5.28 | 4.86 | 5.59 |
| 3,3-DM pentane | 0.00 | 0.00 | 0.00 |
| 2-M hexane | 0.83 | 0.84 | 0.88 |
| 3-M hexane | 0.31 | 0.31 | 0.34 |
| 3-Ethyl pentane | 0.00 | 0.00 | 0.00 |
| *n*-Heptane | 0.00 | 0.00 | 0.00 |
| Distribution of C8 (wt%) | 53.20 | 44.31 | 51.92 |
| 2,2,3-TMP | 0.40 | 0.23 | 0.45 |
| 2,2,4-TMP | 22.05 | 15.84 | 21.25 |
| 2,3,3-TMP | 4.91 | 3.39 | 5.54 |
| 2,3,4-TMP | 10.84 | 10.03 | 11.04 |
| 2,2-DMH | 0.09 | 0.09 | 0.08 |
| 2,3-DMH | 5.65 | 5.32 | 5.32 |
| 2,4-DMH | 4.37 | 4.40 | 3.76 |
| 2,5-DMH | 4.19 | 4.33 | 3.72 |
| 3,3-DMH | 0.00 | 0.00 | 0.00 |
| 3,4-DMH | 0.50 | 0.48 | 0.49 |
| 2-MH | 0.00 | 0.00 | 0.00 |
| 3-MH | 0.00 | 0.00 | 0.00 |
| 4-MH | 0.00 | 0.00 | 0.00 |
| 3-E,2-M pentane | 0.20 | 0.21 | 0.27 |
| C5–C8 olefins | 0.84 | 1.02 | 0.64 |
| C9+ | 13.70 | 23.82 | 10.40 |

*Note.* Reactions were performed at 80°C and 300 psi ($WHSV_{olefin} = 0.1\ h^{-1}$, $i/o_{molar}$ ratios = 98). Time on stream, 5 min.

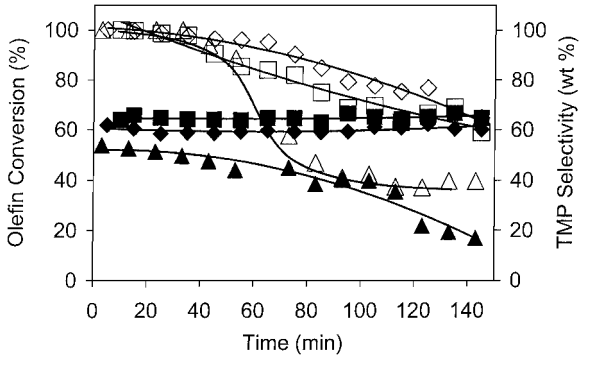


**FIG. 9.** Olefin conversion (open symbols) and TMP selectivity (closed symbols) for L-3.5 (◇, ◆), L-6.5 (□, ■), and L-20 (△, ▲). Reactions were performed at 80°C and 300 psi ($WHSV_{olefin} = 0.1\ h^{-1}$, $i/o_{molar} = 98$).

**TABLE 8**

**Initial Product Selectivity of Individual Compounds Obtained over LTL Samples**

| Samples | L-3.5 | L-6.5 | L-20 |
|---|---|---|---|
| 2-Butene conversion (wt%) | 100.00 | 100.00 | 100.00 |
| *n*-Butane (wt%) | 4.45 | 4.23 | 2.38 |
| Distribution of C5 (wt%) | 6.79 | 7.01 | 10.58 |
| 2-Methyl butane | 6.79 | 7.01 | 10.58 |
| *n*-Pentane | 0.00 | 0.00 | 0.00 |
| Distribution of C6 (wt%) | 3.55 | 3.79 | 4.14 |
| 2,2-DM butane | 0.00 | 0.00 | 0.00 |
| 2,3-DM butane | 2.36 | 2.19 | 2.39 |
| 2-M pentane | 0.59 | 0.80 | 0.73 |
| 3-M pentane | 0.61 | 0.79 | 1.01 |
| *n*-Hexane | 0.00 | 0.00 | 0.00 |
| Distribution of C7 (wt%) | 7.65 | 6.66 | 6.94 |
| 2,2,3-TM butane | 0.12 | 0.09 | 0.11 |
| 2,2-DM pentane | 0.00 | 0.00 | 0.00 |
| 2,3-DM pentane | 3.82 | 3.22 | 3.15 |
| 2,4-DM pentane | 3.03 | 2.63 | 2.62 |
| 3,3-DM pentane | 0.00 | 0.00 | 0.00 |
| 2-M hexane | 0.29 | 0.33 | 0.50 |
| 3-M hexane | 0.40 | 0.38 | 0.56 |
| 3-Ethyl pentane | 0.00 | 0.00 | 0.00 |
| *n*-Heptane | 0.00 | 0.00 | 0.00 |
| Distribution of C8 (wt%) | 73.56 | 75.29 | 65.42 |
| 2,2,3-TMP | 2.18 | 4.52 | 2.84 |
| 2,2,4-TMP | 15.77 | 23.12 | 15.12 |
| 2,3,3-TMP | 11.96 | 10.86 | 10.55 |
| 2,3,4-TMP | 31.84 | 25.40 | 25.25 |
| 2,2-DMH | 0.00 | 0.04 | 0.00 |
| 2,3-DMH | 4.92 | 4.61 | 4.50 |
| 2,4-DMH | 2.83 | 3.21 | 2.99 |
| 2,5-DMH | 0.92 | 1.57 | 1.16 |
| 3,3-DMH | 0.00 | 0.00 | 0.00 |
| 3.4-DMH | 2.68 | 1.65 | 2.64 |
| 2-MH | 0.00 | 0.00 | 0.00 |
| 3-MH | 0.00 | 0.00 | 0.00 |
| 4-MH | 0.00 | 0.00 | 0.00 |
| 3-E,2-M pentane | 0.46 | 0.31 | 0.36 |
| C5–C8 olefins | 0.33 | 0.41 | 0.73 |
| C9+ | 3.66 | 2.61 | 9.81 |

*Note.* Reactions were performed at 80°C and 300 psi ($WHSV_{olefin} = 0.1\ h^{-1}$, $i/o_{molar}$ ratios = 98). Time on stream: L-3.5, 5 min; L-6.5, 10 min; L-20, 3 min.

behavior is the specific pore structure of LTL (aperture of 7.1 Å) connected with large void spaces (aperture of 12.6 Å)) that allows the formation of the bulky trimethylpentane carbenium ions. Furthermore, the inherently high Al content provides a high capacity for HTR, thereby reducing the amount of unsaturated compounds in the product stream. For the LTL samples with the highest aluminum content the lumped selectivities for all the products, especially those for TMPs and DMHs, remained unchanged with respect to time on stream. However, deactivation of the LTL samples was observed since their activity decreased with time.

The L-20 sample initially gave similar conversion and selectivity when compared with the other LTL samples. However, the decrease in C8 paraffins (TMPs and DMHs) to low levels and the subsequent increase in olefins indicates a suppressed HTR capability. This is due to the low aluminum content. Furthermore, the conversion dropped to lower levels than that obtained over the L-3.5 and L-6.5 samples. Again, this is a consequence not only of the low aluminum content but also of the silicate salt deposited in the zeolite during AHF dealumination (28).

The similarity in the TMP distribution between LTL (Table 8) and USY was observed in this study. This indicates that the alkylation reaction takes place inside the channels (7.1-Å pore size with periodic expansions of 12.6 Å) of LTL, which is comparable to the pore of USY (pore size of 7.4 Å and supercages of 13 Å).

### *ZSM-12*

The time-on-stream behavior of ZSM-12 samples of various Si/Al ratios is presented in Fig. 10. The activity of all ZSM-12 samples remained at high levels in comparison with the other zeolites tested, namely USY, mordenite, and L zeolite, under identical operating conditions. These results indicate that ZSM-12 hinders, to a large extent, the formation of carbonaceous compounds. This characteristic of ZSM-12 is of great importance for the development of alkylation catalysts or general refining catalysts that traditionally suffer from coke formation. The stable behavior of ZSM-12 observed in this work was not expected if one considers that it is a one-dimensional zeolite. Previous reports (17) suggest that three-dimensional zeolites should be less susceptible than two- or one-dimensional zeolites to deactivation. Pore plugging is typically anticipated to have only negligible effects on three-dimensional, large-pore zeolites as a consequence of the multiple pathways that the structures offer, whereas pore plugging is thought to occur

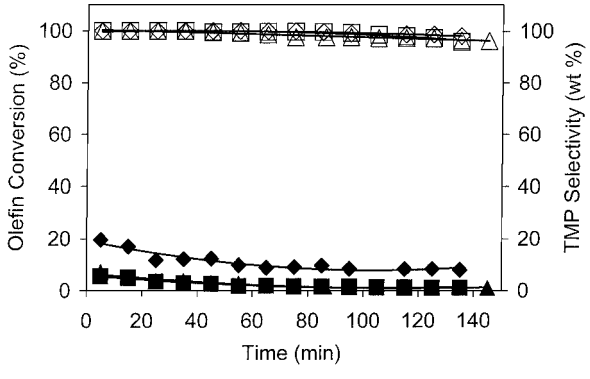


**FIG. 10.** Olefin conversion (open symbols) and TMP selectivity (closed symbols) for Z-38 (◇, ◆), Z-45 (□, ■), and Z-58 (△, ▲). Reactions were performed at 80°C and 300 psi ($WHSV_{olefin} = 0.1\ h^{-1}$, $i/o_{molar} = 98$).

**TABLE 9**

**Initial Product Selectivity of Individual Compounds Obtained over ZSM-12 Samples**

| Samples | Z-38 | Z-45 | Z-58 |
|---|---|---|---|
| 2-Butene conversion (wt%) | 100.00 | 100.00 | 100.00 |
| *n*-Butane (wt%) | 1.07 | 0.78 | 0.54 |
| Distribution of C5 (wt%) | 8.78 | 7.59 | 6.79 |
| 2-Methyl butane | 8.78 | 7.59 | 6.79 |
| *n*-Pentane | 0.00 | 0.00 | 0.00 |
| Distribution of C6 (wt%) | 7.34 | 3.70 | 3.74 |
| 2,2-DM butane | 0.00 | 0.00 | 0.00 |
| 2,3-DM butane | 5.22 | 1.84 | 1.91 |
| 2-M pentane | 1.48 | 1.21 | 1.17 |
| 3-M pentane | 0.64 | 0.65 | 0.66 |
| *n*-Hexane | 0.00 | 0.00 | 0.00 |
| Distribution of C7 (wt%) | 8.85 | 4.40 | 4.76 |
| 2,2,3-TM butane | 0.36 | 0.07 | 0.09 |
| 2,2-DM pentane | 0.00 | 0.00 | 0.00 |
| 2,3-DM pentane | 2.75 | 1.23 | 1.46 |
| 2,4-DM pentane | 4.43 | 1.19 | 1.34 |
| 3,3-DM pentane | 0.00 | 0.05 | 0.19 |
| 2-M hexane | 0.99 | 1.30 | 1.10 |
| 3-M hexane | 0.32 | 0.56 | 0.58 |
| 3-Ethyl pentane | 0.00 | 0.00 | 0.00 |
| *n*-Heptane | 0.00 | 0.00 | 0.00 |
| Distribution of C8 (wt%) | 36.73 | 32.43 | 36.20 |
| 2,2,3-TMP | 0.00 | 0.00 | 0.00 |
| 2,2,4-TMP | 12.16 | 1.85 | 2.47 |
| 2,3,3-TMP | 2.21 | 1.26 | 1.53 |
| 2,3,4-TMP | 5.23 | 2.55 | 3.19 |
| 2,2-DMH | 0.00 | 0.13 | 0.15 |
| 2,3-DMH | 3.82 | 3.99 | 5.35 |
| 2,4-DMH | 4.40 | 5.22 | 6.56 |
| 2,5-DMH | 8.06 | 16.65 | 15.65 |
| 3,3-DMH | 0.01 | 0.09 | 0.30 |
| 3,4-DMH | 0.84 | 0.69 | 1.00 |
| 2-MH | 0.00 | 0.00 | 0.00 |
| 3-MH | 0.00 | 0.00 | 0.00 |
| 4-MH | 0.00 | 0.00 | 0.00 |
| 3-E,2-M pentane | 0.00 | 0.00 | 0.00 |
| C5–C8 olefins | 1.53 | 7.66 | 9.57 |
| C9+ | 35.70 | 43.44 | 38.40 |

*Note.* Reactions were performed at 80°C and 300 psi ($WHSV_{olefin} = 0.1\ h^{-1}$, $i/o_{molar}$ ratios = 98). Time on stream, 5 min.

readily in two- or one-dimensional zeolites. We believe that the remarkable stability of ZSM-12 for this reaction is a result of its pore structure. ZSM-12 possesses one-dimensional noninterpenetrating channels (5.5 × 6.2 Å) which behave as "perfect tubes" and do not lead to the accumulation of coke precursors. Our previous characterizations involving $NH_3$-STPD experiments with fresh and used bifunctional ZSM-12 (20) indicated that even after extensive operation the acid sites of ZSM-12 were practically free of coke. The high stability of ZSM-12 for the alkylation of i-butane with 2-butene (bimolecular reaction) constitutes an extension of our earlier work involving zeolites for monomolecular reactions, namely the hydroconversion of *n*-octane (18) and of branched octanes (19). This behavior renders ZSM-12 a very good candidate for acid-catalyzed reactions suffering from coke formation over a wide range of temperatures. However, it should be mentioned that L zeolite, which is also one dimensional, deactivates very rapidly. This is because the one-dimensional pores of L zeolite consist of apertures of 7.2 Å followed by regions of increased diameter (12.6 Å).

For samples with higher Si/Al ratios the initial TMP selectivites were significantly lower than those observed over Z-38. The low TMP selectivities observed were as expected since the pores of ZSM-12 are more confining (5.6 × 6.2 Å) compared with those of the other zeolites used and do not allow the formation of bulky transition-state intermediates. Moreover, relatively lower hydrogen transfer activity of ZSM-12 samples (see Table 9) due to higher Si/Al ratios yielded the lower amount of TMP isomers.

## CONCLUSIONS

The present study focuses on the impact of structure of selected large-pore zeolites for activity and selectivity during the alkylation of isobutane with 2-butene. The selectivites of TMP isomers, which are primary products from real alkylation, were affected mainly by pore structure. The ratio of 2,2,4-/2,2,3-TMP to 2,3,3,-/2,3,4-TMP at the initial stages of reaction (5 min on stream) decreased in the following order: beta ≥ ZSM-12 > mordenite > USY ≥ LTL. Moreover, one observed comparable trends for the ratio of other major products, 2,5-/2,4-/2,3-DMH to 3,4-DMH. The cracking products (C5–C7) were formed by type A β-scissions from $[C_{12}H_{25}]^+$ and $[C_{16}H_{33}]^+$ cations.

For the activity of olefin conversion, pore structure also plays very important roles. The beta and ZSM-12 samples preserved their activity with time on stream. Under the same operating conditions, USY and mordenite deactivated very fast. This is in direct disagreement with the general notion that higher dimensional structures are capable of resisting deactivation by pore plugging. Their linear channels do not possess any expansions and thus do not allow the formation of bulky carbonaceous materials that could lead to pore plugging.

USY and LTL showed the typical behavior in which more dealuminated samples resulted in faster deactivation with time on stream. This trend mainly resulted from the decreased hydrogen transfer capability because of the lower acid site density. However, the dealumination procedure affected significantly the activity of catalyst. The samples with higher Si/Al ratio (M-35 and B-30) preserved their activity to a better extent than the less dealuminated samples (M-13 and B-26). It is suggested that high hydrogen transfer capability of lower Si/Al zeolites does not guarantee stable activity for this reaction.

## ACKNOWLEDGMENTS

The authors wish to acknowledge the financial support of the National Science Foundation through the CAREER Award (CTS-9702081). Acknowledgment is made to the donors of the Petroleum Research Fund, administered by the ACS, for support of this research through Grant ACS-PRF 31606-G5.

## REFERENCES

1. Corma, A., Martinez, A., and Martinez, C., *J. Catal.* **146**, 185 (1994).
2. Simpson, M. F., Wei, J., and Sundaresan, S., *Ind. Eng. Chem. Res.* **35**, 3861 (1996).
3. De Jong, K. P., Mesters, C. M. A. M., Pfereroen, D. G. R., van Brugge, P. T. M., and de Groot, C., *Chem. Eng. Sci.* **51**, 2053 (1996).
4. Taylor, R. J., and Sherwood, D. E., Jr., *Appl. Catal. A* **155**, 195 (1997).
5. Pater, J., Cardona, F., Canaff, C., Gnep, N. S., Szabo, G., and Guisnet, M., *Ind. Eng. Chem. Res.* **38**, 3822 (1999).
6. Flego, C., Kiricsi, I., Parker, W. O., Jr., and Clerici, M. G., *Appl. Catal. A* **124**, 107 (1995).
7. Juquin, B., Raatz, F., and Marcilly, C., French Patent 2,631,956 Al (1989).
8. Corma, A., Gomez, V., and Martinez, A., *Appl. Catal. A* **119**, 83 (1994).
9. Innes, R. A., Zones, S. I., and Nacamuli, G. J., U.S. Patent 4,891,458 (1990).
10. Chou, T.-S., Huss, A., Jr., and Kennedy, C. R., U.S. Patent 4,992,616 (1991).
11. Nivarthy, G. S., He, Y., Seshan, K., and Lercher, J. A., *J. Catal.* **176**, 192 (1998).
12. Loenders, R., Jacobs, P. A., and Martens, J. A., *J. Catal.* **176**, 545 (1998).
13. Huang, T. J., U.S. Patent 4,384,161 (1983).
14. Chou, T.-S., Huss, A., Jr., and Kennedy, C. R., U.S. Patent 4,918,255 (1990).
15. Husain, A., Huss, A., Jr., and Rahmim, I. I., U.S. Patent 5,475,175 (1995).
16. Blasco, T., Corma, A., Martinez, A., and Martinez-Escolamo, P., *J. Catal.* **177**, 306 (1998).
17. Corma, A., and Martinez, A., *Catal. Rev.–Sci. Eng.* **35**, 483 (1993).
18. Zhang, W., and Smirniotis, P. G., *J. Catal.* **182**, 400 (1999).
19. Zhang, W., and Smirniotis, P. G., *Appl. Catal. A*, submitted.
20. Zhang, W., and Smirniotis, P. G., *Appl. Catal. A* **168**, 113 (1998).
21. Gopal, S., Yoo, K., and Smirniotis, P. G., *Microporous Mesoporous Mater.* **49**, 149 (2001).
22. Robb, G. M., Zhang, W., and Smirniotis, P. G., *Microporous Mesoporous Mater.* **20**, 307 (1998).
23. Zhang, W., Burckle, E. C., and Smirniotis, P. G., *Microporous Mesoporous Mater.* **33**, 173 (1999).
24. Chen, N. Y., Degnan, T. F., and Smith, C. M., "Molecular Transport and Reaction in Zeolites." VCH, New York, 1994.
25. Cardona, F., Gnep, N. S., Guisnet, M., Szabo, G., and Nascimento, P., *Appl. Catal. A* **128**, 250 (1995).
26. Chu, Y. F., and Chester, A. W., *Zeolites* **6**, 195 (1986).
27. Weitkamp, J., and Traa, Y., *in* "Handbook of Hetrogeneous Catalysis" (G. Ertl, H. Knozinger, and J. Weitkamp, Eds.), Vol. 4, p. 2039. VCH, Weinheim, 1997.
28. Chauvin, B., Boulet, M., Massiani, P., Fajula, F., Fiureras, F., and Courieres, T. D., *J. Catal.* **126**, 537 (1990).
29. Querini, C. A., and Roa, E., *Appl. Catal. A* **163**, 205 (1997).
30. Newsam, J. M., *Mater. Res. Bull.* **21**, 661 (1986).